Proceedings of the Czech–Japanese Seminar in Applied Mathematics 2006
Czech Technical University in Prague, September 14-17, 2006
pp. 37–49

CARDIAC MRI DATA SEGMENTATION USING THE PARTIAL DIFFERENTIAL EQUATION OF ALLEN–CAHN TYPE

RADOMÍR CHABINIOK[1,2], JAROSLAV TINTĚRA[2]

Abstract. The work deals with the segmentation of the image data using the algorithm based on the numerical solution of the geometrical evolution partial differential equation of the Allen-Cahn type. This equation has origin in the description of motion by mean curvature and has diffusive character. The diffusion process can be controlled by the input intensity signal, so that edges of the objects or areas can be found. The method is applied to the problem of automated segmentation of the left heart ventricle from the images obtained by magnetic resonance (cardiac MRI). The segmentation is a necessary step for estimation of significant indicators of the myocardial function from dynamic MR images such as the ejection fraction or the kinetic parameters of the wall thickening during the cardiac cycle. These parameters describe clinical situation of the myocardium.

Key words. Image processing, segmentation, PDE, Allen-Cahn equation, cardiac MRI.

AMS subject classifications. 35K15, 35K20, 53A04, 92C50

1. Introduction. Magnetic resonance imaging (MRI) is a modern non-invasive imaging technique used in medicine to produce high quality images of the inside of the human body (see [9]). Development of fast imaging MR sequences allowed the examination of unsteady tissues such as the beating heart (cardiac MRI, see [8]).

Dynamical examination of the heart kinetics stands for a valuable examination of the myocardium. During this examination several hundreds of MR images are measured covering the entire left ventricle volume and recording complete cardiac cycle interval with the temporal resolution of about 40 ms (see Fig. 1.1). Segmentation of the heart ventricle volume and of the wall of the ventricle is an important part of the cardiac MRI data postprocessing (see Fig. 1.2). Hemodynamic parameters such as the ejection fraction, the stroke volume or kinetic parameters of the wall thickening can be estimated from the segmented images. Compared with echocardiography (an usual technique for the heart examination based on ultrasound emission and detection), MRI provides better spatial resolution and allows for quantification of the function of myocardium in a reproducible way. Since the number of images from a single cardiac MRI dynamical examination exceeds 100 (number of slices times number of time frames), automation of the segmentation procedure is necessary. In the presented work we deal with the automated segmentation of the cardiac MR images.

Since most pathologies of the heart in the adulthood are localized in the left heart ventricle (for example the myocardial infarction), we deal with the segmentation of the left heart ventricle with the purpose to interpret its dynamics.

In the following section we give information about the level set formulation of the motion of curves by mean curvature. Then we describe segmentation model from [3] based on the phase–field approach to the mean curvature flow which is used for image segmentation in the presented work. Finally we present results of segmentation of

[1]Mathematical Institute, Faculty of Mathematics and Physics, Charles University in Prague, Czech Republic
[2]MR Unit, Department of Diagnostic and Interventional Radiology, Institute for Clinical and Experimental Medicine, Prague, Czech Republic

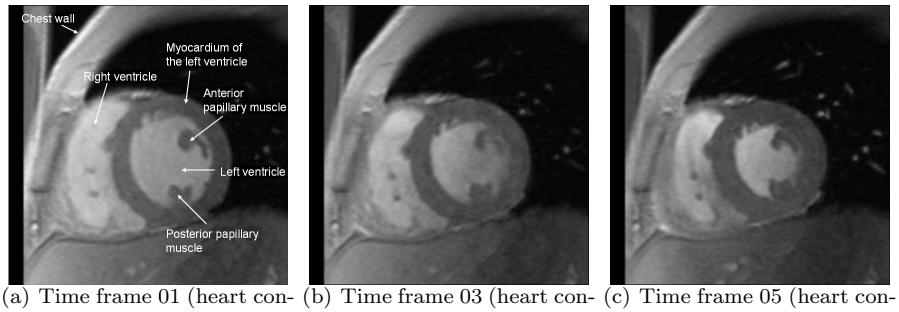

(a) Time frame 01 (heart contraction) (b) Time frame 03 (heart contraction) (c) Time frame 05 (heart contraction)

(d) Time frame 07 (heart contraction) (e) Time frame 09 (heart contraction) (f) Time frame 11 (heart relaxation)

(g) Time frame 13 (heart relaxation) (h) Time frame 15 (heart relaxation) (i) Time frame 17 (heart relaxation)

FIG. 1.1. *Example of cardiac MR images – dynamic CINE series of the heart in short axes (see [7], pages 415-418). A slice corresponding to the mid-cavity part of the ventricle during the cardiac cycle. Time frame 01 corresponds to the end-diastole (maximal ventricle volume), time frame 09 to the end-systole (minimal ventricle volume). Total number of images from single examination exceeds 100. The segmentation procedure has to be proceeded in all the images. For anatomical details see [8], pages 61-83.*

cardiac MR dynamic CINE images using the model.

2. Segmentation by mean curvature flow. Detection of objects boundaries in an image, that are given by the magnitude of the spatial gradient is a known approach to the image segmentation. The level set method is applicable in this problem (see [2, 12, 13]). A segmentation function $u(t,x)$ evolves from the initial condition given by $u(0,x) = u_{ini}(x)$ under a law described by the equation:

$$\frac{\partial u}{\partial t} = |\nabla u| \, \nabla \cdot \left(g(|\nabla u_0|) \frac{\nabla u}{|\nabla u|} \right), \tag{2.1}$$

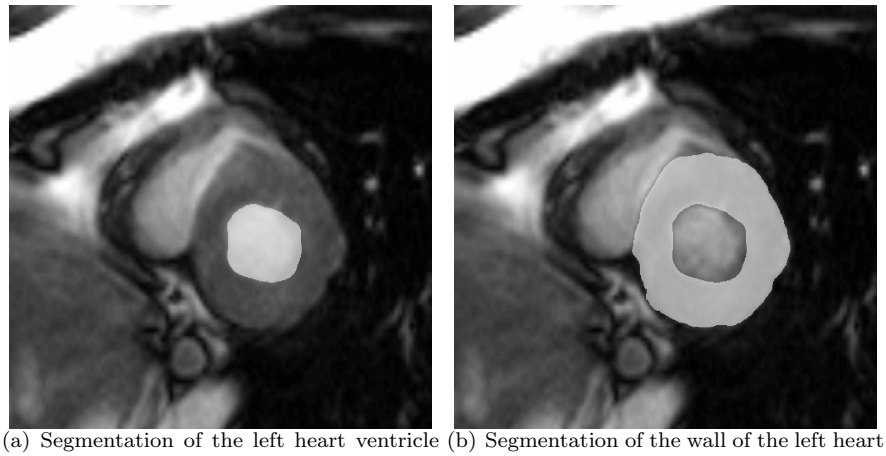

(a) Segmentation of the left heart ventricle volume (b) Segmentation of the wall of the left heart ventricle

FIG. 1.2. *Example of MR images of the heart in short axes. The left ventricle volume and the wall of the left heart ventricle are marked by white color.*

where $u_0(x)$ stands for the input image (intensity of MR signal in the input image), $g : \mathbb{R}_0^+ \to \mathbb{R}^+$ is a non-increasing edge detector function (the Perona–Malik function, see [14]) for which $g(0) > 0$, $g(\sqrt{s})$ is smooth, $g(s) \to 0$ for $s \to +\infty$. The evolution of level sets of the function u according to equation (2.1) can be used to the detection of object boundaries.

We can re-write (2.1) into an advection–diffusion form:

$$\frac{\partial u}{\partial t} = \underbrace{g(|\nabla u_0|)\,|\nabla u|\,\nabla \cdot \left(\frac{\nabla u}{|\nabla u|}\right)}_{(A)} + \underbrace{\nabla g(\nabla |u_0|) \cdot \nabla u}_{(B)}. \tag{2.2}$$

The vector field $-\nabla g(|\nabla u_0|)$ in the advective term (B) in equation (2.2) has an important geometrical meaning. It points towards regions in the image where the magnitude of the spatial gradient of the intensity signal u_0 is large and makes level sets of the segmentation function u concentrate in these areas.

To segment such noisy images like cardiac MR images, the advection itself would not be sufficient. It would lead to detection of spurious edges. The term (A) in equation (2.2) avoids such a false detection. It describes motion by mean curvature. It adds a curvature dependence to the level set flow and regularizes the evolution in the normal direction. Sharp irregularities are smoothed and the curve length in regions with missing edge information is minimized. The process can be also interpreted as an intrinsic diffusion of the curves dependent on $|\nabla u_0|$.

A semi-implicit method of discretization of equation (2.2) using co-volume scheme is described in [12].

3. Edge Detection using Allen–Cahn Equation. In our work we use the algorithm based on the phase–field approach to the mean curvature flow (see [3]). Compared to the segmentation method described in Section 2, we denote the segmentation function by $p(t, x)$. The function $p(t, x)$ evolves according to the modified Allen–Cahn equation (see [1]):

$$\xi \frac{\partial p}{\partial t} = \xi \nabla \cdot (g\,(|\nabla G_\sigma * P_0|)\,\nabla p) + g\,(|\nabla G_\sigma * P_0|)\left(\frac{1}{\xi} f_0(p) + \xi F |\nabla p|\right),$$

$$
\begin{aligned}
&\text{in } (0,T)\times\Omega,\\
p\,|_{\partial\Omega} = 0 \quad &\text{on } (0,T)\times\partial\Omega,\\
p|_{t=0} = p_{ini} \quad &\text{in } \overline{\Omega},
\end{aligned}
\tag{3.1}
$$

where $\Omega = (0, L_1)\times(0, L_2) \subset \mathbb{R}^2$, $L_1 > 0$, $L_2 > 0$ is a rectangular area that represents the input image, $x = [x_1, x_2] \in \Omega$ is a spatial parameter, $t \in (0, T)$ time, $0 < \xi \ll 1$ is a constant parameter (connection to level-set segmentation methods for $\xi \to 0_+$, see Section 4).

The function $p(t, x) \in [0, 1]$ is related to the characteristic function of the segmented area. The boundary of the segmented area in time t matches with the the level set $\{x \in \Omega : p(t, x) = \frac{1}{2}\}$. An initial guess of the segmented area $p(0, x) = p_{ini}(x)$ can be given by:

$$
p(0,x) = p_{ini}(x) = \begin{cases} 1 & \text{for } x \in \text{initial guess of segmented area,}\\ 0 & \text{for } x \in \text{elsewhere,}\end{cases}
$$

(see Fig. 3.1). The automated choice of p_{ini} is discussed in Section 6.

Intensity of the MR signal in the segmented image enters our model by means of the function $P_0(x)$. Values of the input data signal P_0 are between 0 and 255 and can be normalized to the interval $[0, 1]$. Other terms in equation (3.1) are as follows:

- G_σ is Gauss smoothing kernel, $G_\sigma = \frac{1}{(4\pi\sigma)} e^{-\frac{|x|^2}{4\sigma}}$. The convolution with the piecewise constant function P_0 (input digital image) converts P_0 to an infinitely smooth function and also removes some spurious structures (the increase of the signal-to-noise ratio). The convolution is proceeded before the numerical solution of equation (3.1), the convolved input signal is denoted again by P_0.
- $g : \mathbb{R}_0^+ \to \mathbb{R}^+$ is a non-increasing Perona–Malik function (see Section 2). The feature $g(|\nabla P_0|) \to 0$ for $|\nabla P_0| \to +\infty$ makes the diffusion process to stop near edges in the image. Our choice of the Perona–Malik function: $g(s) = \frac{1}{1+\lambda s^2}$, parameter $\lambda > 0$.
- F has meaning of an external force that influences motion of the curves. The sign of F causes either expanding of the segmented area (for $F > 0$) or its shrinking (for $F < 0$).
- f_0 is a polynomial, our choice $f_0(p) = p(1-p)(p-\frac{1}{2})$ is related to the motion of phase–fields by mean curvature (see [6]).

The segmentation function $p(t, x)$ evolves under a diffusion process described by equation (3.1). The diffusion process stops on edges of the objects in the image. Finally after a convenient time T the segmented area p covers the area of our interest (see Fig. 3.2).

The initial–boundary–value problem (3.1) is investigated by means of weak formulation. As usual, we use the notation: $(u, v) = \int_\Omega u(x)v(x)\mathrm{d}x$, $\mathcal{D}(\Omega)$ is a space of infinitively smooth functions with compact support in Ω. In [5], the following statement is proved:

THEOREM 3.1. *Let $p_{ini} \in H_0^1(\Omega)$, then there exists a unique solution of the weak formulation of the initial–boundary–value problem (3.1):*

$$
\begin{aligned}
\xi\frac{\mathrm{d}}{\mathrm{d}t}(p,q) + \xi\Big(g(|\nabla P_0|)\nabla p, \nabla q\Big) &= \frac{1}{\xi}\Big(g(|\nabla P_0|)f_0(p), q\Big) + \xi\Big(g(|\nabla P_0|)F|\nabla p|, q\Big),\\
p(0,x) &= p_{ini}(x),
\end{aligned}
\tag{3.2}
$$

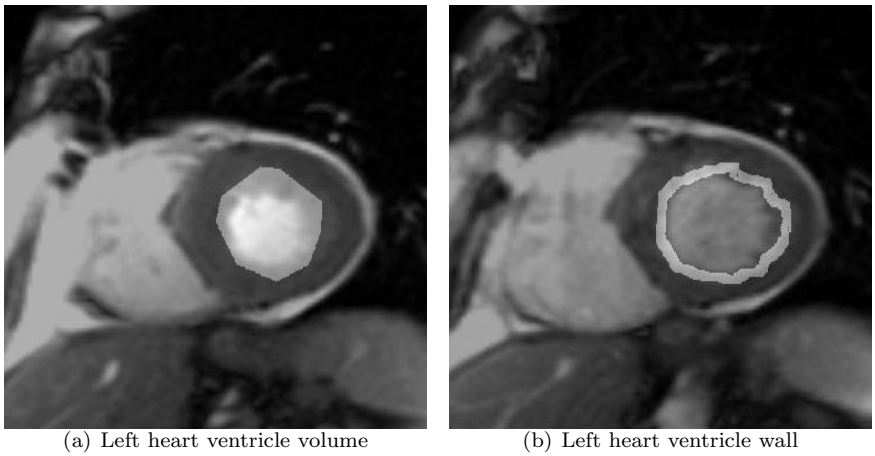

(a) Left heart ventricle volume (b) Left heart ventricle wall

FIG. 3.1. *Examples of the initial guess p_{ini} for the segmentation of the left heart ventricle volume and for the ventricle wall segmentation.*

a.e. $t \in (0,T)$, $\forall x \in \Omega, \forall q \in \mathcal{D}(\Omega)$, *which satisfies:*

$$p \in L^2\left(0,T;H^2\left(\Omega\right) \cap H_0^1\left(\Omega\right)\right),$$
$$\frac{\partial p}{\partial t} \in L^2\left(0,T;L^2\left(\Omega\right)\right).$$

4. Relationship to level-set methods. In this section we briefly describe connection of the equation (3.1) to level–set methods. More detailed description is in [4]. The mean–curvature flow can be expressed by a law from differential geometry

$$v_\Gamma = -\kappa_\Gamma + F, \tag{4.1}$$

where v_Γ stands for a velocity of a motion of a closed curve Γ in $\mathbb{R}^2$, κ_Γ is a curvature of Γ and F has meaning of an external force that influences the motion. This is a central law for reasoning the segmenting models from Sections 2 and 3.

Describing the motion of the level set $\Gamma(t) = \{x \in \Omega : p(t,x) = 0\}$ under the law given by the equation (4.1), using the notation:

A normal to the level set Γ	...	$\vec{n_\Gamma} = -\frac{\nabla p}{\lvert\nabla p\rvert}$,
a normal velocity to the level set Γ	...	$v_\Gamma = \frac{1}{\lvert\nabla p\rvert} \cdot \frac{\partial p}{\partial t}$,
the mean curvature of Γ	...	$\kappa_\Gamma = \nabla \cdot (\vec{n_\Gamma}) = -\nabla \cdot \frac{\nabla p}{\lvert\nabla p\rvert}$.

We obtain a level set equation:

$$\frac{\partial p}{\partial t} = \lvert\nabla p\rvert \nabla \cdot \frac{\nabla p}{\lvert\nabla p\rvert} + F, \tag{4.2}$$

which describes mean curvature flow of level sets. The segmenting model (2.1) from Section 2 is based on the equation (4.2).

Now, the Allen–Cahn equation (3.1) in a context of the law described by (4.2):

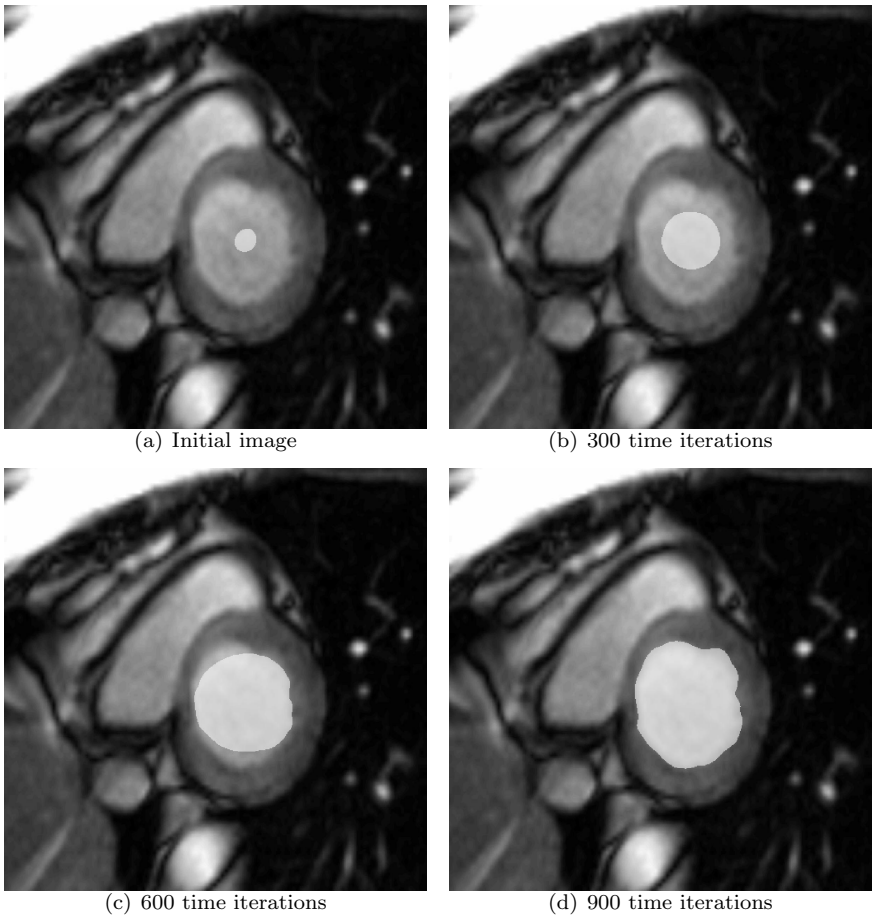

(a) Initial image (b) 300 time iterations

(c) 600 time iterations (d) 900 time iterations

FIG. 3.2. *Evolution of the initial area p_{ini} according to equation (3.1). Parameters of equation (3.1): $\xi = 0.09$, $\lambda = 0.0005$ ($\lambda_{norm} = 30$ for P_0 normalized to the interval $[0, 1]$), $F = 2$, time step $\tau = 0.005$. The process can be viewed as a nonlinear diffusion dependent on a magnitude of the spatial gradient of the input image ($|\nabla P_0|$).*

For $\xi \to 0_+$ the level set $\Gamma(t) = \{x \in \Omega : p(t, x) = \frac{1}{2}\}$ is evolving under a law of the mean–curvature flow. Connection of the problem (3.1) to the law described by the equation (4.1) for $\xi \to 0_+$ can be expressed by the scheme:

$$\begin{array}{ccccccc} \underbrace{\xi \frac{\partial p}{\partial t}} & = & \underbrace{\xi \nabla \cdot (\nabla p) + \frac{1}{\xi} f_0(p)} & + & \underbrace{\xi F |\nabla p|}. \\ \downarrow & & \downarrow & & \downarrow \\ v_\Gamma & = & -\kappa_\Gamma & + & F \end{array}$$

5. Numerical scheme. The discretization is designed according to [3]. We approximate the initial–boundary–value problem (3.1) on a rectangular grid that corresponds with the initial image (MR image of size 512 x 512 pixels). Each picture element has a corresponding node in this grid. For the refinement of the grid we use

bilinear interpolation of the initial picture data. Next, we describe a semi-implicit[1] numerical scheme in a finite difference formulation[2].

We discretize problem (3.1) in space and time on a regular rectangular grid:

$$\begin{aligned}\overline{\omega_n} &= \{[ih_1, jh_2] : i = 0, \ldots, N_1; \quad j = 0, \ldots, N_2\}, \\ \omega_n &= \{[ih_1, jh_2] : i = 0, \ldots, N_1 - 1; \quad j = 0, \ldots, N_2 - 1\}.\end{aligned}$$

Notation:

τ	...	the time step,
h_1, h_2	...	mesh sizes,
N_1, N_2	...	number of grids in respective directions,
$p_{i,j}^k$	...	value of $p(x,t)$ in the node $x = [ih_1, jh_2]$, in time $t = k\tau$.

Discretization of the variables:

$$\begin{aligned}\tfrac{\partial p}{\partial t}|_{t=k\tau} &\to \tfrac{p^k - p^{k-1}}{\tau}, \\ \nabla p|_{i,j}^k &\to \left(\tfrac{p_{i+1,j}^k - p_{i,j}^k}{h_1}, \tfrac{p_{i,j+1}^k - p_{i,j}^k}{h_2}\right), \\ \bar{\nabla} p|_{i,j}^k &\to \left(\tfrac{p_{i,j}^k - p_{i-1,j}^k}{h_1}, \tfrac{p_{i,j}^k - p_{i,j-1}^k}{h_2}\right), \\ (\nabla \cdot q)|_{i,j} &\to \left(\tfrac{q_{i+1,j}^1 - q_{i,j}^1}{h_1} + \tfrac{q_{i,j+1}^2 - q_{i,j}^2}{h_2}\right), \quad \text{where} \quad q = (q^1, q^2).\end{aligned}$$

After the discretization we get a system of nonlinear algebraic equation, that can be written in the form:

$$\xi \mathbf{A}\mathbf{p} - \frac{\tau}{\xi}\mathbf{f}(\mathbf{p}) = \xi \mathbf{F}, \tag{5.1}$$

where

$$\begin{aligned}\mathbf{p} &= \left(p_{i,j}^k\right)_{i=1,j=1}^{N_1-1,N_2-1}, \\ \mathbf{A}\mathbf{p} &= \left(p_{i,j}^k - \tau \nabla \cdot \left(g \bar{\nabla} p^k\right)_{i,j}\right)_{i=1,j=1}^{N_1-1,N_2-1}, \\ \mathbf{f}(\mathbf{p}) &= \left(g_{i,j} f_0\left(p_{i,j}^k\right)\right)_{i=1,j=1}^{N_1-1,N_2-1}, \\ \mathbf{F} &= \left(p_{i,j}^{k-1} + \tau g_{i,j} F_{i,j} \left|\left(\bar{\nabla} p^{k-1}\right)_{i,j}\right|\right)_{i=1,j=1}^{N_1-1,N_2-1}.\end{aligned}$$

We decompose a linear operator $\mathbf{A}$ into diagonal operator, lower and upper triangular operators, so that $\mathbf{A} = \mathbf{D} + \mathbf{L} + \mathbf{U}$.

$$\begin{aligned}\mathbf{D}\mathbf{p} &= \left(p_{i,j}^k + \tau\left(\frac{g_{i+1,j} + g_{i,j}}{h_1^2} + \frac{g_{i,j+1} + g_{i,j}}{h_2^2}\right) p_{i,j}^k\right)_{i=1,j=1}^{N_1-1,N_2-1}, \\ \mathbf{L}\mathbf{p} &= \left(-\tau \frac{g_{i,j}}{h_1^2} p_{i-1,j}^k - \tau \frac{g_{i,j}}{h_2^2} p_{i,j-1}^k\right)_{i=1,j=1}^{N_1-1,N_2-1}, \\ \mathbf{U}\mathbf{p} &= \left(-\tau \frac{g_{i+1,j}}{h_1^2} p_{i+1,j}^k - \tau \frac{g_{i,j+1}}{h_2^2} p_{i,j+1}^k\right)_{i=1,j=1}^{N_1-1,N_2-1}.\end{aligned}$$

[1] Semi-implicitness in sense that nonlinear terms of the equation are treated from the previous time step, the linear terms are considered on the current time level.

[2] Finite elements scheme is practically identical, for easy implementation we are describing the scheme based on finite differences.

We solve (5.1) using Gauss-Seidel nonlinear iterative method in the form:

$$\xi(\mathbf{D}+\mathbf{L})\mathbf{p}^{l+1} = \xi\mathbf{F} - \left(\xi\mathbf{U}\mathbf{p}^{l} - \frac{\tau}{\xi}\mathbf{f}(\mathbf{p}^{l})\right), \tag{5.2}$$

where the index l denotes number of the Gauss-Seidel iteration. For the initial guess we choose the previous time level:

$$\mathbf{p}^0 = \left(p_{i,j}^{k-1}\right)_{i=1,j=1}^{N_1-1,N_2-1}.$$

The size of the mesh either exactly corresponds with the size of the input MR image or we use bilinear interpolation for the mesh refinement.

6. Results. We implemented segmentation algorithm from Section 5 in the C language. The user interface is written in MATLAB. Presenting results were obtained using cardiac MR images of volunteers and patients from MR departments of hospitals IKEM[3] Prague, Na Homolce[4] Prague and Hradec Králové[5].

6.1. Segmentation of the left heart ventricle volume. We segment the volume of the ventricle throughout the systolic and diastolic phase[6] of the cardiac cycle in an automated way.

For every image (slices and time frames) we use initial segmented area p_{ini} that covers the whole ventricle volume (see Figs. 3.1(a) and 6.1(a)). The cross-section of the heart ventricle is decreasing from the heart base to its apex and it is decreasing also during the systolic phase of the cardiac cycle. Using these facts we derive p_{ini} for the actual image automatically from the segmented neighbouring image (either in time or spatial domain), so that p_{ini} covers the whole heart volume.

For the parameter $F < 0$ the automatically given area p_{ini} shrinks. Its movement stops on the edge representing the inner contour of the ventricle, so that the left heart ventricle volume in one image is segmented.

After the volume segmentation we can describe the dynamics of the ventricle volume by summing the segmented areas all over the left heart ventricle (see Figs. 6.2 and 6.3). From these values for example a global parameter of heart contractility – *ejection fraction of the ventricle* (EF) – can be estimated. Definition of the ejection fraction of the heart is: EF = (EDV − ESV)/EDV, where EDV means end-diastolic volume of the ventricle, ESV means end-systolic volume of the ventricle (see [11]).

Normal EF is between 55% and 80%. Pathologically lower value may be a sign of cardiac insufficiency. It comes along with ischemic heart disease (IHD) and its complications, heart inflammation, dilated cardiomyopathy, etc. Cardiac MRI is used as a reference method for estimation of EF.

6.2. Segmentation of the wall of the left heart ventricle. The initial segmented area p_{ini} for the segmentation of the ventricle wall is derived automatically from the segmented ventricle volume (see Fig. 3.1(b) – by a small expansion of the segmented volume area). Then the area p_{ini} is evolving under the equation (3.1) with the parameter $F > 0$ that causes expansion of the area. We fix $p(t, x) = 0$ inside the ventricle volume.

[3] `http://www.ikem.cz/`
[4] `http://www.homolka.cz/en/`
[5] `http://www.fnhk.cz/`
[6] Systole – period of the myocardial contraction, diastole – period of ventricle filling.

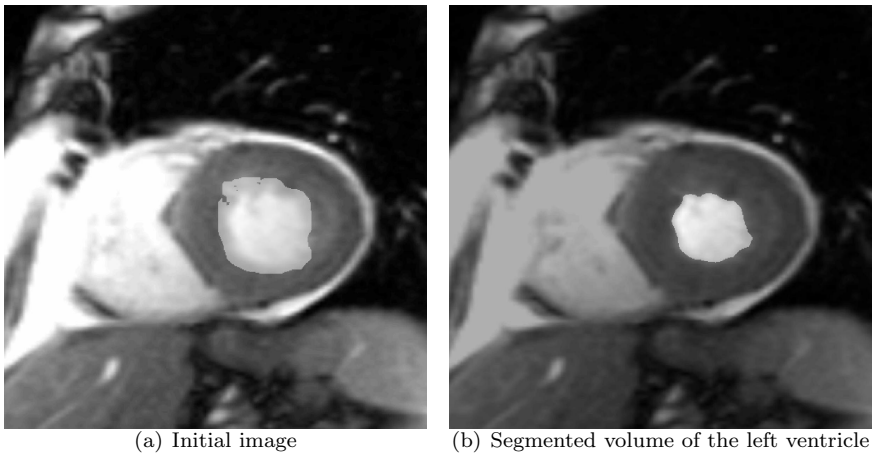

(a) Initial image (b) Segmented volume of the left ventricle

FIG. 6.1. *Example of the left heart ventricle segmentation. A slice corresponding to the basal part of the ventricle. Time frame 07 (corresponding to the end-systole). On the left p_{ini} automatically derived from the previous time image, on the right result of the segmentation. Parameters of equation (3.1): $\xi = 0.09$, $\lambda = 0.0005$ ($\lambda_{norm} = 30$), $F = -1$, time step $\tau = 0.005$. Number of time iterations: 200.*

Our algorithm is less successful compare to the ventricle volume segmentation. Although more manual corrections have to be performed, Figs. 6.4 and 6.5 show promising results of the application of the model to the wall segmentation[7].

From the segmented ventricle wall, local parameters of the wall thickening in radial direction during the cardiac cycle can be estimated. These are local parameters of the myocardial kinetics. For the proper interpretation, the left ventricle is divided into 17 segments according to the convention of *the American Heart Association Writing Group on Myocardial Segmentation and Registration for Cardiac Imaging* (see [10]). The thickening of the normokinetic myocardium during the cardiac cycle is greater than 30% (see Figs. 6.6 and 6.7).

7. Discussion. Cardiac MRI data segmentation is an important part of the MR data post-processing. In our case the number of acquired images from single examination is about 200. This number is too high to segment images manually. However, the data character of cardiac MR images (such as limited signal-to-noise and contrast-to-noise ratio, motion and pulsation artifacts) makes the automated segmentation to be a rather difficult task.

An algorithm for medical data segmentation has to be successful in detection of objects in the image and also it has to be fast enough, so that clinical physicians would benefit from its usage. Currently on a 2GHz PC, our algorithm segments the ventricle volume in one image in about 20 seconds (using the numerical grid with 300×300 degrees of freedom, time step $\tau = 0.01$, 300 time iterations).

In the presented work we also dealt with non-constant choice of parameters λ and F in the equation (3.1). We tried to choose these parameters with respect to the non-constant signal-to-noise ratio in the images[8]. Although we prefer data acquisition with

[7] These results were obtained using images acquired by so called 'trueFISP' MR sequence (denoted also as 'balanced SSFP', see [7], pages 579-606) that provides good signal-to-noise ratio. Unfortunately, for the MR sequence 'FLASH' (see [7], pages 415-418) the results are not so good.

[8] It is caused e.g. by signal inhomogeneities resulting from different level of signal detection by

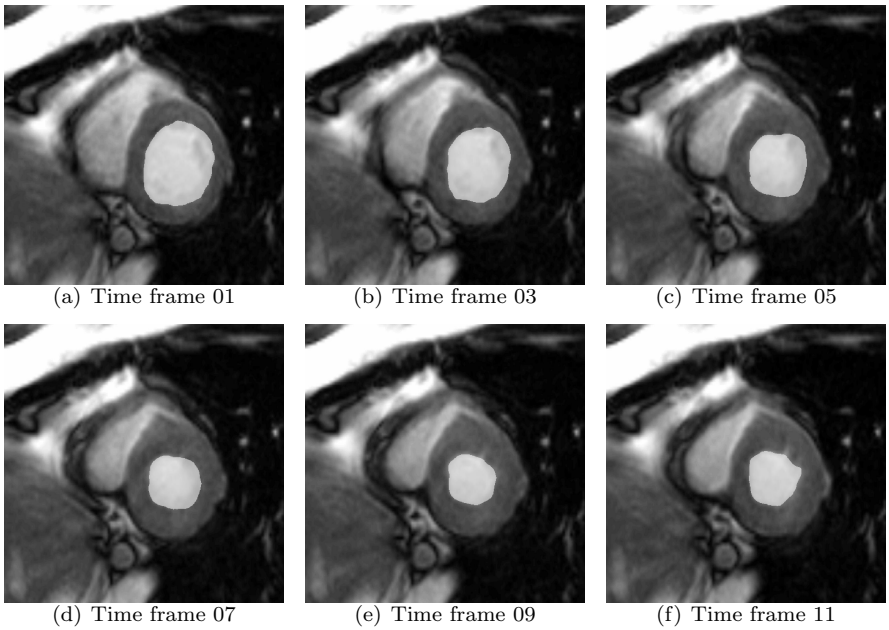

(a) Time frame 01 (b) Time frame 03 (c) Time frame 05

(d) Time frame 07 (e) Time frame 09 (f) Time frame 11

FIG. 6.2. *Example of the left heart ventricle segmentation. A slice corresponding to the basal part of the ventricle. Time frames 01 – 10 correspond to the period of contraction of the ventricles (systole), time frames 11 – 15 to the period of the filling of the ventricles (diastole). Parameters of equation (3.1):* $\xi = 0.09$, $\lambda = 0.0005$ *(*$\lambda_{norm} = 30$*),* $F = -1$, *time step* $\tau = 0.005$. *Number of time iterations: 200.*

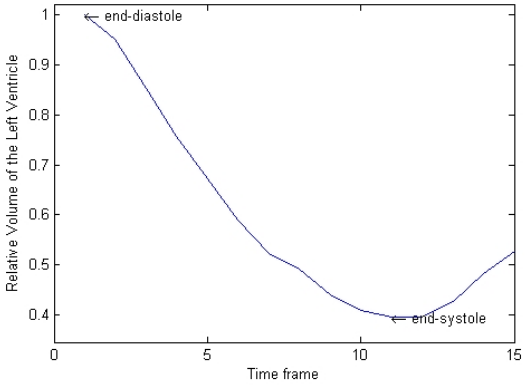

FIG. 6.3. *Graph of relative volume of the left ventricle versus time during the cardiac cycle. The ejection fraction (EF) is about 60%, that is a normal value.*

the quality as high as possible, the modification e.g. with external force F dependent on an input signal P_0 is promising.

Choice of the stopping time of the evolution depends on other parameters of equation (3.1) (namely λ, F, ξ, h, τ). Usual approach is to terminate the evolution when the change of the segmentation function p is below a specified threshold. Due to

acquisition coils of the MR system in different spatial localization.

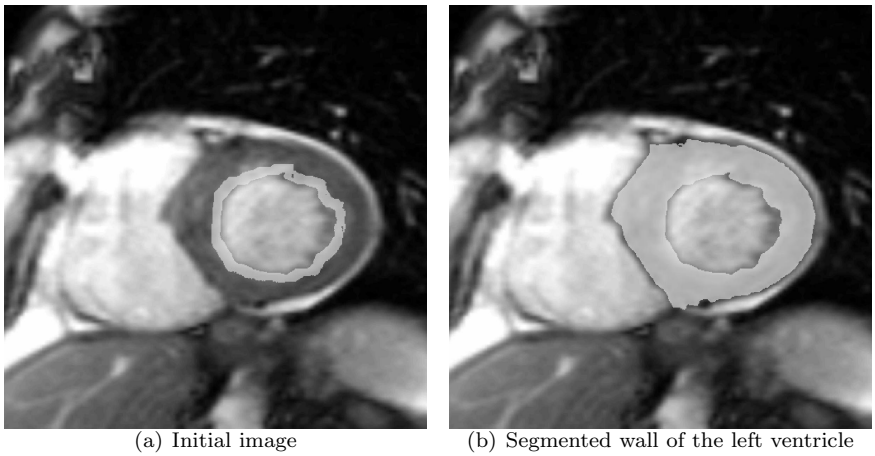

(a) Initial image (b) Segmented wall of the left ventricle

FIG. 6.4. *Example of the left heart ventricle wall segmentation. Time frame 01 (corresponding to the end-diastole). On the left p_{ini}, on the right result of the segmentation. Parameters of equation (3.1): $\xi = 0.09$, $\lambda = 0.0005$ ($\lambda_{norm} = 30$), $F = 2$, time step $\tau = 0.005$. Number of time iterations: 400.*

many irregularities in our images we choose a fixed number of iteration. We estimate this number in the first segmented image and then use this value for the segmentation of all other images in this examination.

In future new techniques in MRI will certainly make possible to get cardiac MR dynamic images with better spatial and temporal resolution. Number of commonly acquired images from a single examination may rise to thousands. Then an automation of the procedure of the heart segmentation will be a fundamental part of data acquisition.

Images with better spatial and temporal resolution might even improve the diagnostic possibilities. For example cardiac pathologies could be better localized, the heart function could be better described using e.g. cardiac stress–strain model, fluid–structure interaction, etc. The description as exact as possible is important for the indication of proper treatment modalities.

8. Conclusion. In our work we successfully adapted the segmentation model described in [3] to the problem of cardiac MRI data segmentation. Our algorithm is successful in automated segmentation of the heart ventricle volumes and wall of the left heart ventricle (with eventual minor manual correction). The goal of our work is an automated algorithm for image processing helpful in clinical examinations.

9. Acknowledgment. This work was supported by the project MŠMT LC06052 (Nečas Center for Mathematical Modeling) and by grants MSMT 1M6798582302, MZO 00023001, Czech Republic. Authors thank to MR departments of hospitals IKEM Prague, Na Homolce Prague and Hradec Králové for providing MR image data.

REFERENCES

[1] S. ALLEN, AND J.W. CAHN, *A Microscopic Theory for Antiphase Boundary Motion and its Application to Antiphase Domain Coarsening*, Acta Metall. **27** (1979), 1084–1095.

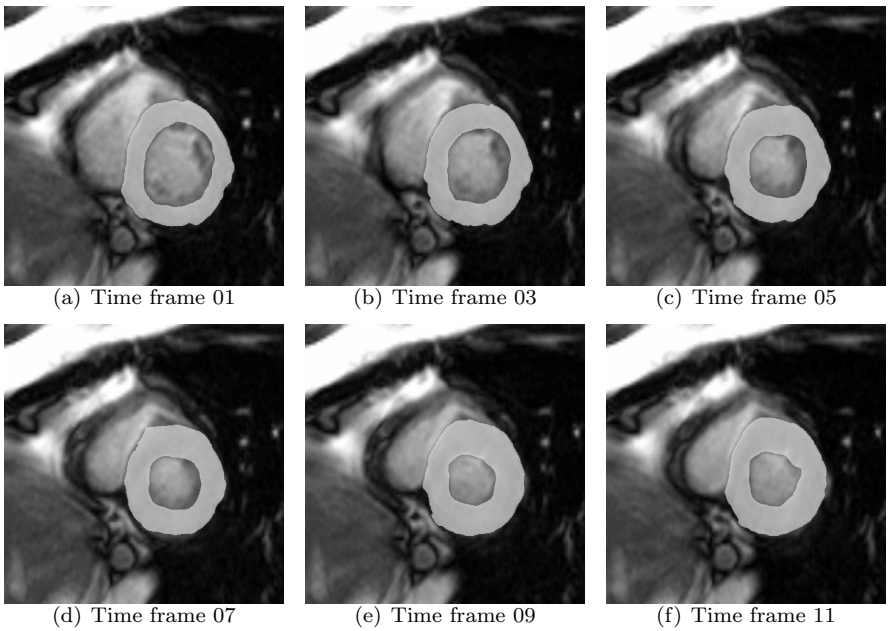

(a) Time frame 01 (b) Time frame 03 (c) Time frame 05

(d) Time frame 07 (e) Time frame 09 (f) Time frame 11

FIG. 6.5. *Example of the left heart ventricle wall segmentation. Slice corresponding to the basal part of the ventricle, succession from the end-diastole to the end-systole. Parameters of equation (3.1):* $\xi = 0.09$, $\lambda = 0.0005$ ($\lambda_{norm} = 30$), $F = 2$, *time step* $\tau = 0.005$. *Number of time iterations: 400.*

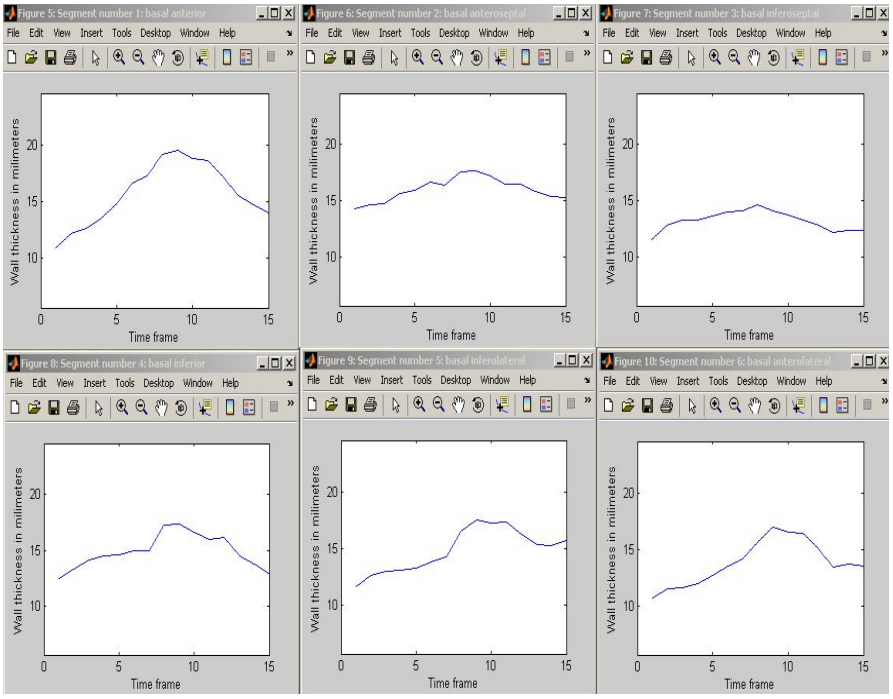

FIG. 6.6. *Wall thickness versus time graph during the cardiac cycle estimated from the slice depicted in Fig. 6.5.*

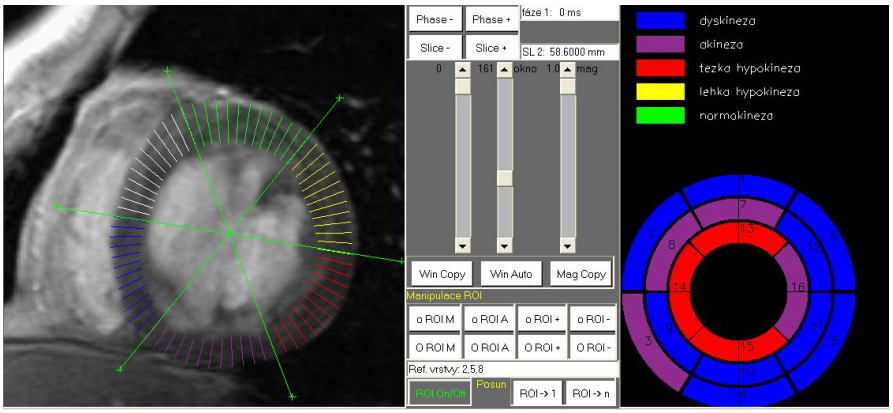

FIG. 6.7. *An example of the wall kinetics estimation. Result of the examination of the patient with severe myocardial dysfunction. On the left a measurement of the wall thickening from the segmented wall of the left heart ventricle. On the right a 17-segment polar map of the left heart ventricle myocardium according to [10]. Color scale from blue – dyskinetic myocardium, purple – akinetic myocardium, red – severe hypokinetic myocardium to green color – normokinetic myocardium.*

[2] G. AUBERT, AND P. KORNPROBST, *Mathematical Problems in Image Processing*, Springer-Verlag, New York (2002).

[3] M. BENEŠ, V. CHALUPECKÝ, AND K. MIKULA, *Geometrical Image Segmentation by the Allen-Cahn Equation*, Applied Numerical Mathematics **51**, no. 2 (2004), 187–205.

[4] M. BENEŠ, *Diffuse-Interface Treatment of the Anisotropic Mean–Curvature Flow*, Appl. Math. **48**, no. 6 (2003), 437–453.

[5] M. BENEŠ, *Mathematical Analysis of Phase–Field Equations with Numerically Efficient Coupling Terms*, Interfaces and Free Boundaries **3** (2001), 201–221.

[6] M. BENEŠ, *Numerical Simulation of Microstructure Growth in Solidification*, Habilitation Thesis, Faculty of Nuclear Sciences and Physical Engineering, Czech Technical University in Prague, 2002 (in Czech).

[7] M.A. BERNSTEIN, K.F. KING, AND X.J. ZHOU, *Handbook of MRI Pulse Sequences*, Elsevier (2004).

[8] J. BOGAERT, S. DYMARKOWSKI, AND A.M. TAYLOR, *Clinical Cardiac MRI*, Springer-Verlag, Berlin Heidelberg (2005).

[9] Z. LIANG, AND P.C. LAUTERBUR, *Principles of Magnetic Resonance Imaging*, Institute of Electrical and Eloctronics Engineers, Inc. 3 Park Avenue, New York (2000).

[10] M.D. CERQUEIRA, N.J. WEISSMAN, V. DILSIZIAN ET AL., *Standardized Myocardial Segmentation and Nomenclature for Tomographic Imaging of the Heart: A Statement of Healthcare Professionals from the Cardiac Imaging Comittee of the Council on Clinical Cardiology of the American Heart Association*, Circulation **105** (2002), 539–542.

[11] A.C. GUYTON, AND E.H. HALL, *Textbook of Medical Physiology,* 10^{th} *ed.*, W. B. Saunders Company, 2000, pages 96–262.

[12] K. MIKULA, A. SARTI, AND F. SGALLARI, *Co-Volume Level Set Method in Subjective Surface Based Medical Image Segmentation*, book chapter in *Handbook of Medical Image Analysis: Segmentation and Registration Models*, (J.Suri et al., Eds.), Springer, New York, 2005, pp. 583–626.

[13] S. OSHER, AND R. FEDKIW, *Level Set Methods and Dynamic Implicit Surfaces*, Springer Verlag, New York, 2003.

[14] P. PERONA, AND J. MALIK, *Scale Space and Edge Detection Using Anisotropic Diffusion*, IEEE Trans. Pattern Anal. Mach. Intell. **12** (1990), 629–639.